JGR Space Physics

RESEARCH ARTICLE
10.1029/2020JA028401

Gravity and Pressure-Gradient Currents Using Ionospheric Electron Density Measurements From COSMIC Satellites

J. Sreelakshmi[1] and Geeta Vichare[1]

[1]Indian Institute of Geomagnetism, Navi Mumbai, India

Key Points:
- COSMIC data have limitations in obtaining good latitudinal coverage of plasma densities on a given day at a fixed local time and longitude
- The magnetic field variations due to gravity and pressure-gradient currents increase with solar flux and reduce with altitude
- These effects are stronger at equator to low-latitude region and in the noon to evening sector and negligible in other local time sectors

Supporting Information:
- Supporting Information S1
- Table S1

Correspondence to:
J. Sreelakshmi,
sreelaxmij@gmail.com

Citation:
Sreelakshmi, J., & Vichare, G. (2020). Gravity and pressure-gradient currents using ionospheric electron density measurements from COSMIC satellites. *Journal of Geophysical Research: Space Physics*, *125*, e2020JA028401. https://doi.org/10.1029/2020JA028401

Received 24 JUN 2020
Accepted 1 OCT 2020
Accepted article online 9 OCT 2020

Abstract The gravity-driven and pressure-gradient currents coexist in the ionosphere, and their effects are significant in there, rather than at the outside of the ionosphere; and can be important while studying the ionospheric currents using low-Earth-orbiting (LEO) satellite measurements. Maute and Richmond (2017, https://doi.org/10.1002/2017JA024841) (MR17) have demonstrated that above the *F* region peak, directions of these two coexisting currents are opposite and the net magnetic effects along the ambient magnetic field are nonsignificant. In the view of the diamagnetic corrections being applied to the LEO magnetic field measurements to account for the pressure-gradient currents, it is imperative to examine the proposition of MR17. In the present paper, we have estimated the gravity and pressure-gradient currents, using altitude profiles of electron density obtained from the Constellation Observing System for Meteorology, Ionosphere, and Climate (COSMIC)-1 satellite cluster. In order to get the latitudinal profiles of magnetic field variations at a fixed local time (LT) using COSMIC data, it is required to combine either different days at a fixed longitude or all the longitudes on a fixed day, thus compromising with either days or longitudes. It is found that the net magnetic field is significant in the low-latitude region, which increases with solar flux and decreases with altitude. The magnetic field effects show strong LT dependence and are significant in the noon to evening sector. The comparison of the present estimates with the diamagnetic corrections emphasizes that correcting for only one current can introduce unviable errors and thus supports the suggestion of MR17.

Plain Language Summary In addition to the ionospheric-dynamo currents, the currents due to gravity and plasma pressure-gradients flow in the Earth's ionosphere, whose contribution in the ground magnetic field measurements is negligible compared to that of ionospheric-dynamo. However, considering the magnetic field due to gravity and pressure-gradient currents present in the ionosphere may be important while studying the ionospheric currents using low-Earth-orbiting (LEO) satellite measurements. Above the *F* region peak where LEO satellites generally fly, the directions of these two coexisting currents are opposite and the net magnetic field along the ambient magnetic field is nonsignificant. In the view of the diamagnetic corrections being applied to the LEO magnetic field measurements to account for the pressure-gradient currents, it is imperative to compute the magnetic field effects of these currents using actual observations of ionospheric electron densities. In the present paper, we have estimated the gravity and pressure-gradient currents, using altitude profiles of electron density obtained from the Constellation Observing System for Meteorology, Ionosphere, and Climate (COSMIC)-1 satellite cluster. The magnetic variations due to these currents are estimated at different heights, latitudes, solar fluxes, and local times.

1. Introduction

The high-precision magnetic field measured by several low-Earth-orbiting (LEO) satellite missions has been used successfully to study the Earth's main magnetic field, crustal field, and external field due to ionospheric and magnetospheric currents. During geomagnetic quiet conditions, the daytime ionospheric wind dynamo producing ionospheric currents is the major source of the external field. Several researchers have studied the equatorial electrojet (EEJ) (Jadhav et al., 2002a; Lühr et al., 2004), counter electrojet (CEJ) (Singh et al., 2018; Vichare & Rajaram, 2011), and Sq current systems (Chulliat et al., 2016; Maeda, 1981; Sugiura & Hagan, 1979). However, as the LEO satellites fly in the source region of currents such as gravity-driven currents (GC) and plasma pressure-gradient currents (PC), the contribution due to

these currents can be significant at LEO orbits. Therefore, it is necessary to know their estimates while studying ionospheric-dynamo current and modeling weak lithospheric geomagnetic fields.

The current density in the ionosphere due to various sources can be expressed as (Alken et al., 2017)

$$\boldsymbol{J} = \sigma \boldsymbol{E} + \boldsymbol{J}_w + \boldsymbol{J}_g + \boldsymbol{J}_p \tag{1}$$

$$\boldsymbol{J}_w = \sigma \boldsymbol{U} \times \boldsymbol{B} \tag{2}$$

$$\boldsymbol{J}_g = \frac{n m_i}{B^2} \boldsymbol{g} \times \boldsymbol{B} \tag{3}$$

$$\boldsymbol{J}_p = -\frac{1}{B^2} \nabla P \times \boldsymbol{B} \tag{4}$$

$$\text{where, plasma pressure,} \quad P = nk(T_i + T_e) \tag{5}$$

$\boldsymbol{J}_w$, $\boldsymbol{J}_g$, and $\boldsymbol{J}_p$ are the source currents due to wind dynamo, gravity, and pressure-gradients respectively. $\boldsymbol{E}$ is the electric field, $\boldsymbol{g}$ is the acceleration due to gravity, and $\boldsymbol{B}$ is Earth's magnetic field. The σ is ionospheric conductivity, n is plasma number density, and m_i is ion mass. T_i and T_e are ion and electron temperatures, respectively and k is the Boltzmann constant.

It is clear from the above equations that, in addition to ambient magnetic field $\boldsymbol{B}$, the computation of $\boldsymbol{J}_g$ needs the information about plasma number density, gravity, and m_i; whereas $\boldsymbol{J}_p$ needs gradients in the plasma number density, T_i, and T_e. Considering the significant vertical gradients in the plasma density, knowledge about them is needed to compute $\boldsymbol{J}_p$. Moreover, to estimate the magnetic field signatures due to these currents, the entire height profile of electron density in the ionosphere along with plasma temperatures and ion masses is required, which is not possible to obtain at each point along the satellite traverses. Therefore, it is challenging to determine these currents and associated magnetic field variations. With the diamagnetic assumptions, Lühr et al. (2003) proposed the equation to estimate PC. If the plasma pressure-gradients are not very sharp in quasi-stationary plasma, then the sum of the magnetic pressure and plasma pressure tends to be constant. Thus, based on the quasi-stationary assumption, every increase in plasma pressure has to be counterbalanced by a reduction in the magnetic pressure. Applying linear perturbation approach, the magnetic field variations b due to diamagnetic effect, estimated by Lühr et al. (2003) is

$$b = nk(T_i + T_e)\frac{\mu_0}{B} \tag{6}$$

where μ_0 is the permeability of free space. Lühr et al. (2003) showed the presence of PC during nighttimes using CHAMP satellite magnetic measurements. They showed that some of the features such as local undulations present in the latitudinal profile of the residual fields of LEO data disappear after applying the diamagnetic correction and also the amplitudes of EEJ change considerably. Therefore, to study EEJ or F region currents using LEO satellite magnetic field data, the above correction has been used widely (Lühr & Maus, 2006; Lühr et al., 2004; Manoj et al., 2006). Few more studies are in the literature about GC and PC (Alken et al., 2017; Lühr et al., 2002; Maus & Lühr, 2006) and found that these currents are predominant in the equatorial ionization anomaly (EIA) region (Alken et al., 2011). Using magnetic field measurements from CHAMP and Swarm satellites, Alken (2016) showed the presence of GC. He investigated the seasonal and local time (between 19 and 24 LT) dependence of magnetic field variations; and found that they are strongest during spring/fall, which agrees with the seasonal behavior of the EIA, and continues until midnight, even under solar minimum conditions. The GCs are eastward and significant at low latitudes, as the magnetic field is mostly northward. Maus and Lühr (2006) estimated GC by assuming the intensity of the nondivergent part of GC is controlled by the nighttime current density perpendicular to the magnetic field and the divergent part is inhibited through the induced electric fields. They suggested a need for correcting LEO data for GC and demonstrated through the POMME-3 model. However, these corrections are no longer applied to current geomagnetic field models due to ambiguous current closure assumption (Hulot et al., 2015; Maus et al., 2008).

Maute and Richmond (2017) have used the Thermosphere-Ionosphere-Electrodynamics General-Circulation-Model (TIE-GCM) with an updated electrodynamo module to estimate these currents and

examined their combined effects, as both these currents coexist in the ionosphere. According to them, correcting LEO magnetic observations only for either current without considering the effect of the other will introduce larger errors, as, at the altitudes above *F* region peak, the magnetic effects due to these currents are opposite. Our motive is to examine the proposition of Maute and Richmond (2017) using actual observational data. This is very important as plenty of magnetic field data are getting generated through ongoing three-satellite Swarm mission, which is being utilized for the study of ionospheric currents (Chulliat et al., 2016; Thomas et al., 2017) and modeling of lithospheric fields (Thébault et al., 2017).

For this purpose, the information of the height profiles of electron density is required, which is obtained from Constellation Observing System for Meteorology, Ionosphere, and Climate (COSMIC) satellites. The other required parameters such as m_i, $T_{i,}$ and T_e are obtained from the International Reference Ionosphere (IRI) (Bilitza et al., 2017) model. The objective of the present study is to obtain the magnetic field contributions due to PC and GC in the magnetic field recordings of polar LEO satellites such as Swarm mission satellites, and hence it would be desirable to obtain the latitudinal profile of the magnetic field variations using COSMIC satellite electron density, rather than using model-based estimates.

Section 2 describes the ionospheric electron density data and related instruments of COSMIC satellite cluster, distribution of occultation points in the latitude-longitude frame, and the methodology used to obtain the GC and PC from COSMIC data and associated magnetic field variations. The results obtained at a single occultation point and also the latitudinal profiles of these variations obtained using different approaches are described in section 3. The subsections display the solar flux and LT dependences of these variations. The results are discussed in section 4 and concluded in section 5.

2. Data and Methodology

The GC and PC given by Equations 3 and 4 generate induced electric fields and Pedersen currents, to maintain the divergence-free currents. These secondary currents due to induced electric fields usually flow in the daytime *E* region or the lower *F* region during nighttimes and hence are mostly infinitesimal at the *F* region altitudes. Thus, in the *F* region, where LEO satellites orbit around the Earth, the expressions for $\boldsymbol{J}_g$ and $\boldsymbol{J}_p$, given by Equations 3 and 4 hold good. According to Equations 3 and 4, computation of GC and PC requires the information of electron density, its gradients, plasma temperatures, and ion masses. In the present study, the ion compositions (O^+, NO^+, $O_2{}^+$, and N^+), electron and ion temperatures at various altitudes in the ionosphere are taken from IRI 2016 model (Bilitza et al., 2017) whereas Earth's magnetic field is taken from CHAOS model (Finlay et al., 2016) of the geomagnetic field.

For calculating the magnetic field perturbations due to GC at the observation height "*h*", Maute and Richmond (2017) proposed the following expression:

$$\Delta B_g(h) = \mu_0 \cos I \int_h^{h_{top}} \boldsymbol{J}_g(h')dh' \tag{7}$$

where h_{top} is the upper boundary of the ionosphere, where current becomes zero, and *I* is the inclination of the observation point. Expression 7 is based on the approximation of a one-dimensional current sheet with zero height-integrated current, which produces no magnetic field variations above and below the sheet, but nonzero magnetic perturbations within the sheet. This approximation is valid as the eastward $\boldsymbol{J}_g$ flowing in the *F* region is largely balanced by westward induced currents flowing in the dayside *E* region or nightside lower *F* region. Furthermore, this approximation is simpler to calculate than the solution using the full three-dimensional Biot-Savart relation.

Similarly, the magnetic variations due to plasma pressure-gradient current are

$$\Delta B_p(h) = \mu_0 \cos I \int_h^{h_{top}} \boldsymbol{J}_p(h\prime)dh\prime \tag{8}$$

Note that Equations 7 and 8 give estimates of the perturbation in the scalar magnetic field (the component of the vector perturbation parallel to the ambient magnetic field, *B*) and that the current density used in 7 and 8 is the component in the magnetic-eastward direction. It is clear from the Equations 7 and 8 that

for the computation of magnetic field variations, the entire vertical profile of electron density and its vertical gradients are required.

The vertical profiles of ionospheric electron density measurements obtained from COSMIC/FORMOSAT-3 mission are utilized to estimate the GC and PC. FORMOSAT-3/COSMIC is a constellation of six microsatellites launched on 15 April 2006, into six different orbits at 700–800 km above the Earth's surface at an inclination of 72°. The longitudinal separation between two consecutive satellite orbits is 30° (Cheng et al., 2006). This LEO constellation receives signals transmitted by the 24 U.S. GPS satellites and provides around 2,500 global occultation data per day, distributed all over the globe.

The primary science instrument in COSMIC is GPS Occultation Experiment (GOX) or Integrated GPS Occultation Receiver (IGOR), which provides the height profiles of the ionospheric electron density (Rocken et al., 2004). A detailed description of the inversion technique applied to invert the COSMIC occultation soundings to ionospheric electron density profiles can be found in Schreiner et al. (2007). Abel inversion technique (AIT) is widely used in GPS ionospheric radio occultation (IRO). There have been several efforts to develop and validate IRO retrieval techniques for obtaining the profiles of ionospheric electron densities more accurately (Pedatella et al., 2015; Tulasi Ram et al., 2016). See https://directory.eoportal.org/web/eoportal/satellite-missions/content/-/article/formosat-3 for the details of the COSMIC mission and data. The latitudinal, longitudinal, and LT coverage by COSMIC mission on 27 September 2014 is depicted in Figure S1 in the supporting information. The local time is shown by color bar. It can be observed from the figure that within a longitudinal bin of width ~20–30°, occultation points are covering a good range of the geographic latitudes, but the LTs are very different. Since the motive of the study is to obtain the magnetic field contributions due to these currents in the magnetic observations of polar LEO satellites, it is required to get the latitudinal profile of these estimates. For our analysis latitudinal spacing of around 5° to 8° is required for obtaining the latitudinal profile of currents. Since PC and GC are significant at lower latitudes, the latitudinal coverage from 40°S to 40°N is of particular interest. And in this latitudinal region, the COSMIC data is sparsely available (>10° spacing) at a given longitudinal and LT range. Therefore, the standard patterns of the plasma densities such as EIA in the latitude-altitude frame are not reproduced properly, missing the EIA features. This may put a limitation in obtaining a latitudinal profile of $\boldsymbol{J}_g$ and $\boldsymbol{J}_p$ at a particular longitude and LT as required by high-inclination LEO satellites' trajectories. We overcome this difficulty by adopting following two approaches: One is by considering different days to get the latitudinal profiles at a fixed longitude and LT, and the other approach is considering all the longitudes on a given day and LT. Certainly, it is not appropriate to include all the LTs on a given day, as the latitudinal profiles have strong LT dependence. It may be fair to include all the longitudes on a given day or different days with fixed longitude. The estimates of GC and PC along with associated magnetic field variations using these two approaches are presented in the following sections.

3. Results Using COSMIC Data

3.1. Single Profile

Before estimating the latitudinal profiles of GC and PC and the associated magnetic field variations as required by LEO satellites, we first compute the estimates using the electron density profile at a single occultation point, that is, at a fixed geographic latitude, longitude, and LT. We have selected the vertical profile of electron density collected at two occultation points, corresponding to 15 and 20 LT at 29°S and 15°S geographic latitude respectively, and at ~300°E longitude, during high solar flux ($F10.7 = 182.2$ *sfu*) on 27 September 2014. Since the previous studies (Alken, 2016; Alken et al., 2011; Lühr et al., 2002) have reported that these currents show a strong dependence on the EIA, we focus on 15 and 20 LT, considering EIA normally develops and peaks at these times. Also, Maute and Richmond (2017) have computed these estimates at these LTs and hence it would ease the direct comparison with the numerical model-based results. The COSMIC electron density profile, estimated zonal currents and magnetic field variations are shown in Figure 1. It can be observed that at both the LTs, the GC is positive i.e. eastward at all altitudes. As the electron density peaks at an altitude of ~340–360 km for both the local times, $\boldsymbol{J}_g$ also peaks at ~350 km, with a magnitude of ~20–30 nA/m^2. PCs are eastward in the lower ionosphere (peaks ~250 km) and westward in the *F* region (peaks ~400 km). We compare these results with those of Maute and Richmond (2017) obtained at 300°E longitude and high solar flux ($F10.7 = 200$ *sfu*). Note that their Figures 11-1a and 11-2a represent the

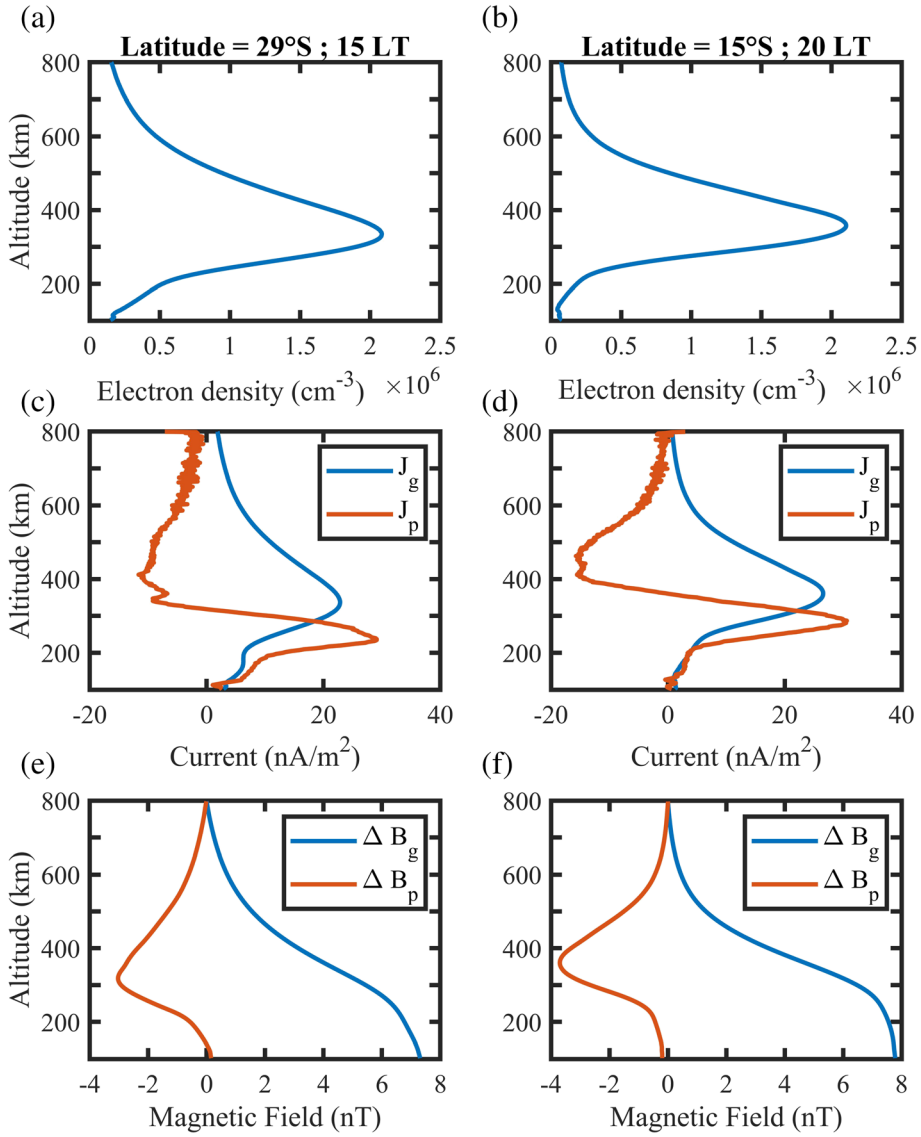

Figure 1. The altitudinal profiles during 27 September 2014 ($F10.7$ = 182.2 *sfu*) at 300°E longitude (a and b) electron density, (c and d) gravity-driven (blue) and plasma pressure-gradient (red) currents at 15 and 20 LT, respectively; (e and f) corresponding magnetic field variations. The geographic latitudes of left and right side plots are 29°S and 15°S, respectively.

GCs obtained using basic equation (i.e., Equation 3), without considering 3-D current system inclusive of induced electric fields. Their results show that $\boldsymbol{J}_g$ peaks at ~450 km and ~20°S with an amplitude of ~20–30 nA/m^2, which are consistent with our results, although there is a difference of 100 km in the height of the peak. Figures 11-1b and 11-2b from Maute and Richmond (2017) display the geographic latitude-altitude profiles of ΔB_g due to source currents without induced parts at 15 and 20 LT, respectively. Though the currents and related magnetic fields in the latitude-altitude frame will be shown and discussed later in the paper, here we compare our results obtained through single profiles. Figure 1 indicates ΔB_g is northward and stronger at lower altitudes with amplitudes of ~7–8 nT, which is similar to that obtained by Maute and Richmond (2017). Though Maute and Richmond (2017) have not explicitly displayed the PC and associated magnetic field perturbations due to the source current alone, they have shown the results obtained by combining the source current with that due to the associated electric fields, in their Figures 3 and 4. It is found that the ΔB_p obtained here is also in qualitative agreement with their

results being southward at higher altitudes, but there is some difference in the magnitude and the height of peak southward field, which may be due to the differences in the solar fluxes. Our results show southward ΔB_p maximizes at ~300–350 km with an amplitude of ~−3 nT (−2 to −4 nT), whereas their computations show a peak at ~450 km with an amplitude of ~−6 to −7 nT. In general, the GC and PC and associated magnetic field variations obtained using COSMIC data qualitatively match with those produced by Maute and Richmond (2017).

3.2. Latitude-Altitude Frame at a Fixed Longitude

The polar (high-inclination) LEO satellite passes through almost all the latitudes along its orbit and have almost a constant LT near lower latitudes. Therefore, to estimate the contributions of these currents at LEO altitudes, it is required to know the latitudinal profile of these estimates at a fixed LT. As depicted in Figure S1, it is not possible to have good latitudinal coverage for a fixed LT using COSMIC occultation points, until we either include different days to get the variation at a fixed longitude or include all the available longitudes on a single day. In this subsection, we fix the longitude and collect the electron density profiles from different days. While combining various days, we tried to group days with similar properties such as season, solar flux, etc. The quiet days (Kp $\leq$ 3+) from equinox months (February, March, September, and October) during years 2014–2018 with high solar flux ($F10.7 = 180 - 200$ *sfu*) were chosen. We set a window of ±0.5 hr in the vicinity of a given LT, that is, considered all the LTs within ±0.5 hr. The longitudinal bin size is chosen as 20°, so that for 300°E, all the longitudes with 300 ± 10° are considered. In the case where more number density profiles in the latitudinal bin of width 8°exist, then the mean values are considered. The values are further interpolated to get the latitudinal resolution of 5°.

Figure 2a and 2b shows the electron density variations in the geographic latitude-altitude frame for longitude 300°E at 15 and 20 LT, during high solar flux conditions. At 15 LT, two peaks at 20°S and 0° geographic latitudes are observed, which may indicate the formation of EIA with a maximum magnitude of 2.2×10^{-6} cm^{-3}, whereas only one peak at 5°S with a magnitude of 1.5×10^{-6} cm^{-3} is evident at 20 LT. Normally, EIA is present at 20 LT; however, the data collected by COSMIC during the considered days and time show the absence of this feature. Comparison of the present electron density profiles obtained from COSMIC with that from TIE-GCM shown in Figure 5 of Maute and Richmond (2017) reveal differences in terms of magnitude and height of the peak. At 15 LT, magnitude of electron density modeled from TIE-GCM is larger (peak ~4×10^{-6} cm^{-3}) than COSMIC observations (peak ~2.2×10^{-6} cm^{-3}). Furthermore, in TIE-GCM, the height of peak electron density is at ~360 to 460 km and the geographic latitudes of peak densities are ~30°S and 5°N, while the COSMIC observations show the height of the peak at ~300–350 km and ~20°S and the geographic equator. Also, at 20 LT there are differences in the peak magnitude of 2.5×10^{-6} cm^{-3} and an altitude difference of ~50–100 km between TIE-GCM and COSMIC values.

Figure 2c-2n represents the variation of the $\boldsymbol{J}_g$, $\boldsymbol{J}_p$, and combined currents ($\boldsymbol{J}_g + \boldsymbol{J}_p$) and corresponding magnetic field variations with latitude and altitude at 15 and 20 LT. $\boldsymbol{J}_g$ is eastward throughout the region, whereas $\boldsymbol{J}_p$ is mainly westward in the upper ionosphere and eastward in the lower ionosphere. At 15 LT, $\boldsymbol{J}_g$, eastward $\boldsymbol{J}_p$, and ($\boldsymbol{J}_g + \boldsymbol{J}_p$) currents show peaks at ~20°S and near the equator, which correspond to ~10°S and 10°N geomagnetic latitude. Significant eastward $\boldsymbol{J}_g$ is present between 300 and 450 km, with an amplitude of ~20 nA/m^2, whereas $\boldsymbol{J}_p$ is eastward below 300 km (peak value ~25 nA/m^2) and westward at higher altitudes. Thus, $\boldsymbol{J}_g$ and $\boldsymbol{J}_p$ are essentially opposite at higher altitudes above the *F* region peak and hence reduces the net current and its magnetic variations. For 20 LT, EIA type two peak structures are neither seen in the electron density nor in $\boldsymbol{J}_g$, $\boldsymbol{J}_p$, and ($\boldsymbol{J}_g + \boldsymbol{J}_p$). Instead, it shows a single peak at 10°S, which corresponds to the geomagnetic equator. Interestingly, $\boldsymbol{J}_p$ shows peak at 250 km with magnitude of ~70 nA/m^2, which is higher than daytime (15 LT) values. This could be due to the larger vertical gradient in the electron density present at that location at 20 LT

Figures 11-1a and 11-2a of Maute and Richmond (2017) show that at both LTs, $\boldsymbol{J}_g$ peaks at an altitude of ~450 km and ~20°S geographic latitude with an amplitude of ~30–40 nA/m^2, and second peak, which is relatively weaker is seen near the geographic equator. The deviations of our results about the peak height and magnitude from those of Maute and Richmond (2017) can be obvious due to the differences in the electron density profiles discussed above. The net current ($\boldsymbol{J}_g + \boldsymbol{J}_p$) due to source currents displayed in their Figure 12 shows two peaks at lower heights between 300 and 400 km, where southern hemispheric peak at ~20–25°S is

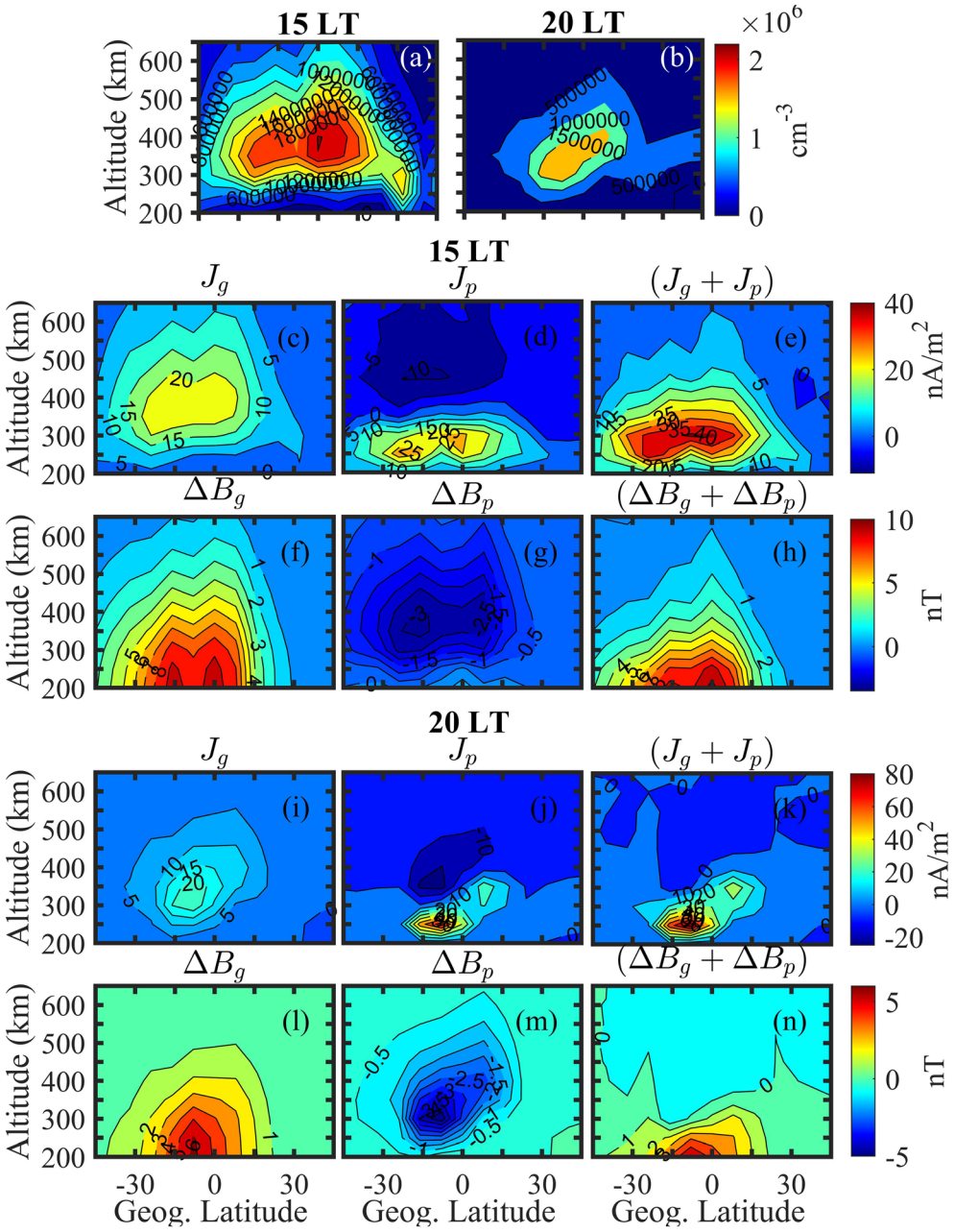

Figure 2. (a) Electron density, (c-e) gravity-driven currents ($\boldsymbol{J}_g$), pressure-gradient currents ($\boldsymbol{J}_p$), and their sum ($\boldsymbol{J}_g + \boldsymbol{J}_p$) and (f–h) their corresponding magnetic perturbations ΔB_g, ΔB_p, and ($\Delta B_g + \Delta B_p$) with geographic latitude and altitude at 300°E geographic longitude, for equinox solar maximum conditions ($180 < F10.7 < 200$) at 15 LT. (b) and (i)–(n) The same as (a) and (c)–(h) respectively, but at 20 LT.

stronger with an amplitude of ~40–50 nA/m^2. Our results at 15 LT (Figures 2c-2h) also show the peaks at lower heights at ~300 km and ~20°S and near the geographic equator; however, the northern peak is slightly stronger in our results.

The ΔB_g is northward and ΔB_p is mainly southward above the $F2$ peak. The ($\Delta B_g + \Delta B_p$) shows significant values at lower heights (below 300 km) and lower latitudes (~10 nT at 15 LT and ~6 nT at 20 LT). At upper altitudes (above 450 km), the combined magnetic effects are less than 2 nT at 15 LT and less than −0.5 nT at 20 LT.

3.3. Solar Flux Dependence

Here, we examine the dependence of the magnetic field variations due to GC and PC on the solar flux. Figure 3 depicts the variations of ΔB_g, ΔB_p and $(\Delta B_g + \Delta B_p)$ with $F10.7$, near 15 LT and at 450 km height, grouped in different latitudinal (magnetic) ranges and are displayed in different subplots. The latitudes are grouped with a range of 5° near the dip equator to lower latitude region, and with a wider range in the mid-latitude region in both the hemispheres, resulting in total nine groups as shown in Figure 3. The southern and northern hemispheric zones are shown on the left and right sides, respectively, while the near-equatorial zone is shown at the bottom. In the figure, the red, blue, and green color symbols represent ΔB_g, ΔB_p, and $(\Delta B_g + \Delta B_p)$, respectively, and corresponding linear fits are also shown with black lines. Two things are evident from the plots: first is that as the solar flux increases, the magnetic field variation due to these currents also increases; second thing is that the magnetic field associated with these currents decreases with latitude and becomes very small beyond 25° latitude. Moreover, as the contributions from ΔB_g and ΔB_p are oppositely directed, the absolute values for $(\Delta B_g + \Delta B_p)$ are smaller than that of ΔB_g or ΔB_p, at an altitude of 450 km. At solar flux of 150 *sfu*, $(\Delta B_g + \Delta B_p)$ is less than 2.5 nT in the equatorial-to-low-latitude region; while in the midlatitudes, it reduces to less than 0.5 nT. As seen from the plots of Figure 3, the slopes of the fitted lines are different at low and middle latitudes. The slope for $(\Delta B_g + \Delta B_p)$ is ~0.02 nT/*sfu* at lower latitudes (<25°), that is, ~2 nT for a change of 100 *sfu*, whereas beyond 25° the slope is nearly 0. The slope for ΔB_p is ~−0.035 and −0.004 nT/*sfu* at low and middle latitudes, respectively. The slope for ΔB_g indicates ~4.5 nT change in ΔB_g at low latitudes and ~0.4 nT change at middle latitudes, with 100 *sfu* change. This may indicate that, the solar flux influence of the magnetic field variations due to GC and PC is considerable at the equatorial-to-low-latitude region and small at midlatitudes.

3.4. Latitude-Altitude Frame on a Single Day

3.4.1. 27 September 2014

In section 3.2, we fixed the longitude and collected different days to obtain the electron density in the latitude-altitude frame. However, in this process, though the longitudinal dependence of the profiles was considered, the day-to-day variability was ignored. For the selected days, the solar flux values and geomagnetic activity index Kp varied from 180 to 200 *sfu* and 0 to 3+, respectively. Thus, even though the data was limited to high solar flux conditions there is still a variability, which can be attributed to the solar flux and geomagnetic variations. In this section, we attempt to address this issue by focusing on 1 day but considering the profiles at all the available longitudes. The distribution of occultation points of the COSMIC constellation on 27 September 2014, in the geographic latitude-LT frame, is displayed in Figure 4a. Again, here we focus on 15 and 20 LT, and the LT windows near these times are shown by horizontal lines, and the points considered are shown by asterisk. For 15 LT sector, we have selected the LTs between 14.3 to 15.5 LT and for 20 LT, the selected bin was slightly wider from 18.8 to 21.4 LT. The determination of this width solely depends on the available points for better latitudinal coverage.

Figures 4b and 4c display the electron density in the dip latitude-altitude frame, for 15 and 20 LT, obtained on 27 September 2014, using the density profiles at the locations indicated in Figure 4a. It should be noted that unlike previous figures, the latitudes are dip latitudes here; as we have considered all the longitudes, it is more appropriate to express the latitudes as dip latitudes rather than geographic latitudes. This is because the offset between geomagnetic and geographic latitude varies significantly with longitude and the plasma density is strongly organized with respect to the magnetic main field. One can notice the density peaks in both hemispheres at ~350–400 km height, for both LT sectors. The dip latitudes of density peaks are at 15°S and 15°N for 15 LT, which may indicate the development of EIA at this time. The locations of density crests are 10°S and 12.5°N for 20 LT, and the peaks are weaker. It seems the electron density profiles obtained here adopting the second approach are more realistic than those obtained through the first approach.

Figures 5a-5f and 5g-5l display the results obtained based on above electron density profiles at 15 and 20 LT, respectively. $\boldsymbol{J}_g$ shows peaks at ~15° dip latitude in both hemispheres for 15 LT, and these positions move equatorward to ~10°S and 5°N for 20 LT sector. $\boldsymbol{J}_p$ and ΔB_p also show two-peak structures at 20 LT, but more clearly at 15 LT. $(\boldsymbol{J}_g + \boldsymbol{J}_p)$ shows peaks at 15°S and 15°N of ~40 nA/m^2 amplitude, near 300 km at 15 LT, whereas the peaks slightly move equatorward at 20 LT, with the strength of ~20 nA/m^2. The combined magnetic field perturbation $(\Delta B_g + \Delta B_p)$ is stronger at the lower heights with some weak two-hemispheric peaks

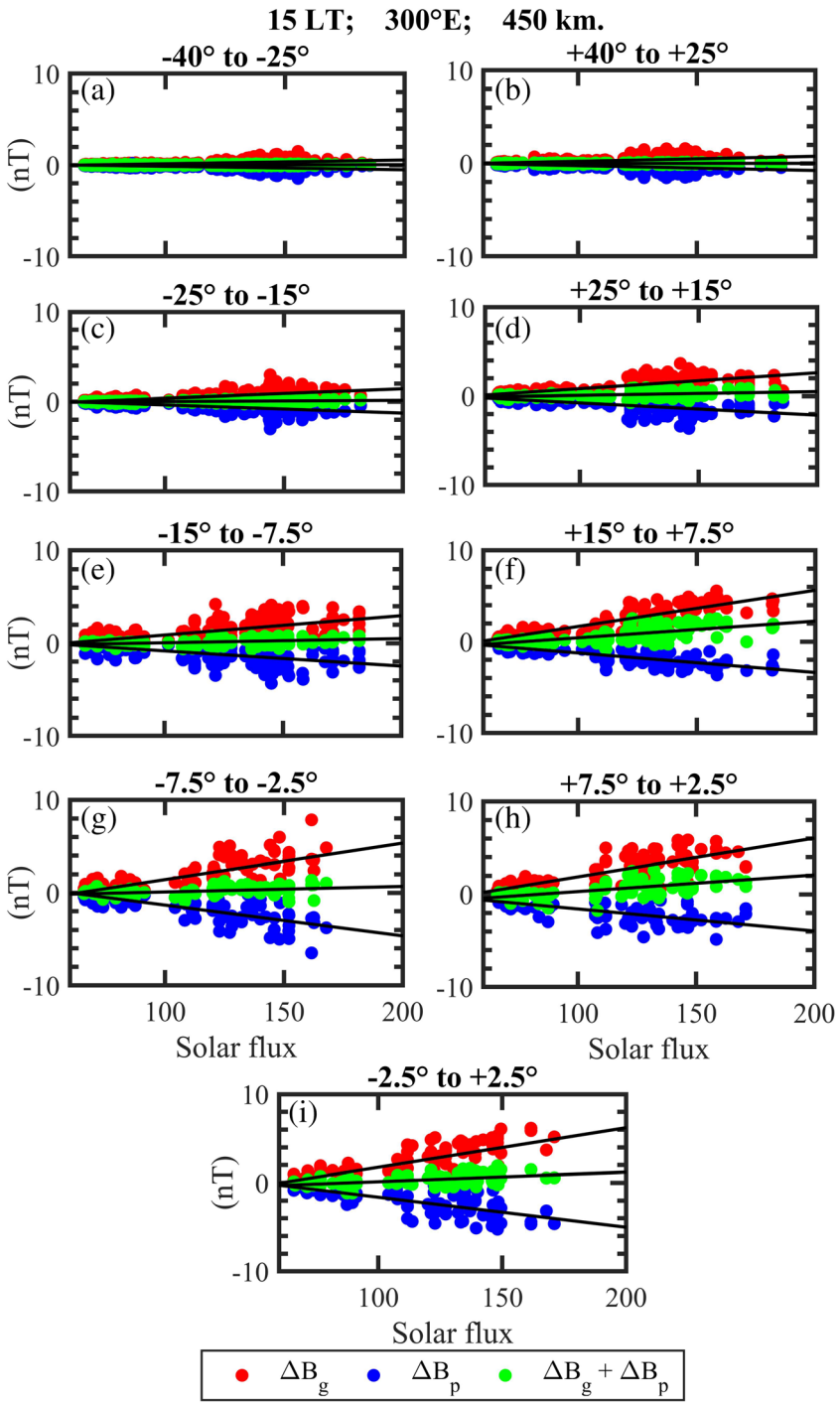

Figure 3. (a–i) Scatter plots of ($\Delta B_g + \Delta B_p$) versus $F10.7$ index, computed at 15 LT, at an altitude of 450 km and geographic longitude of 300°E. The dip latitude range is mentioned at the top of each subplot.

and decreases with height. Comparison of these with those shown in Figure 2c-2n reveals slight differences especially for 20 LT, which could be due to the differences in the electron density profiles; however, the broad features match well particularly for 15 LT sector.

3.4.2. Plausible Effects of Longitudes

The computation of $\boldsymbol{J}_g$ and $\boldsymbol{J}_p$ (Equations 3 and 4) depends on the ($1/B$) factor and also on the latitudes through cosine of inclination factor, in addition to the electron density and its gradients. It is known that the ambient magnetic field is weakest in the American sector (near 300°E longitude) and hence $1/B$ factor

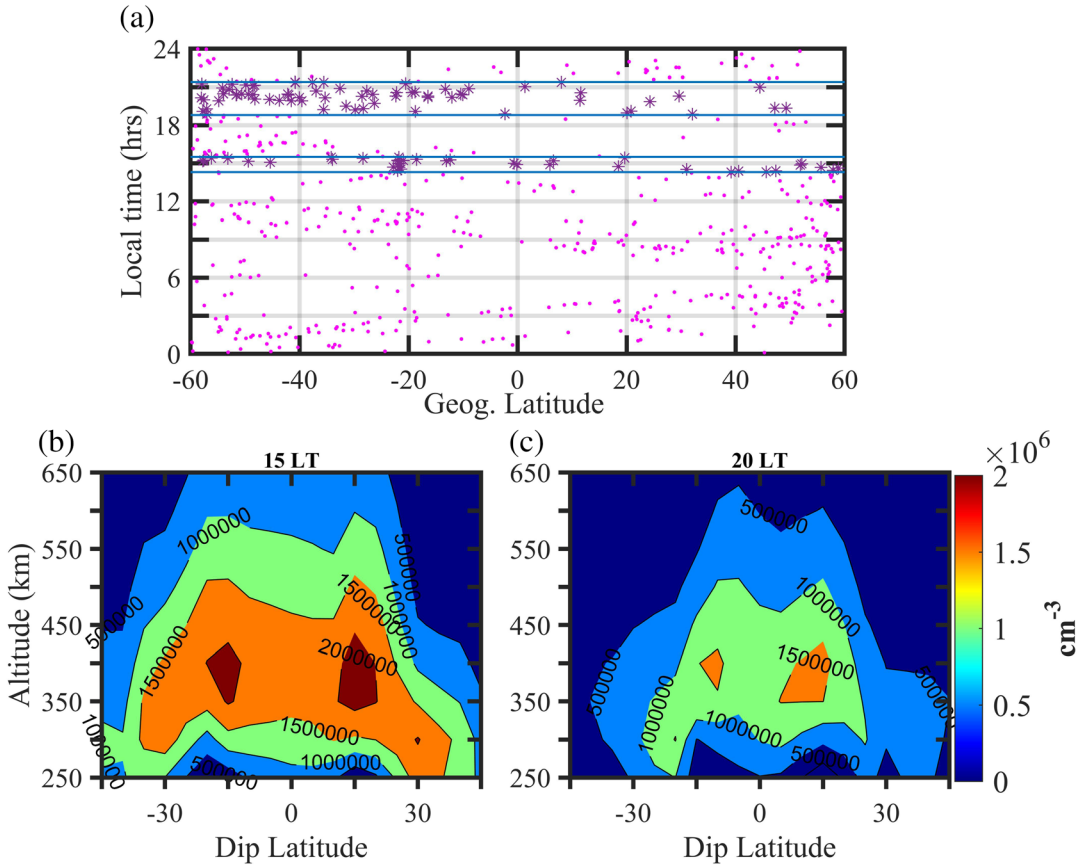

Figure 4. (a) Occultation points of the COSMIC constellation in the latitude-LT frame, on 27 September 2014. The asterisk points represent those corresponding to 15 and 20 LT. (b and c) Electron density at 15 and 20 LT respectively on 27 September 2014 for solar maximum conditions ($F10.7 = 182.2$ *sfu*).

is maximum there (Jadhav et al., 2002b). Figure 6a shows the variation of $(1/B)$ in longitude-dip latitude frame, which is based on the CHAOS model (Finlay et al., 2016) calculations for the year 2014. It shows that there is a differences of ~15,000 T^{-1} between 100°E and 300°E longitudes at the dip equator. Therefore, if the longitudes of the electron density profiles in the COSMIC data vary considerably, especially when the longitudes vary between 100°E and 300°E, then $1/B$ will significantly modify the results depicted above. Figures 6b-6e shows the longitudes along with the latitudinal profiles on different days, selected from September and October months, with local times at 15 hr and 20 hr. The plots indicate that the longitudes vary considerably. Moreover, it is evident from Figure 6 that at 300°E longitude, there are significant latitudinal differences and also there is strong asymmetry about the dip equator position. Therefore, the latitudinal profiles at 300°E may be significantly different than those at other longitudes. Thus, it is clear that the magnitudes of $\boldsymbol{J}_g$, $\boldsymbol{J}_p$, and corresponding magnetic field variations have a strong dependence on the longitudes. Therefore, both the approaches have some limitations in getting the latitudinal profiles of these currents as required for the corrections of LEO observations.

3.5. Local Time Dependence

In this subsection, we examine how the latitudinal profiles of ΔB_g, ΔB_p, and $(\Delta B_g + \Delta B_p)$ vary with LT. We have displayed the results at two altitudes viz., 300 and 450 km. To obtain the LT patterns using the first approach requires a large number of days to have all LTs at fixed longitude. The possibility of getting those many days with high solar flux was examined and found that not sufficient number of days are available, and hence, we adopted the second approach to study the LT dependence.

As seen in Figure 4a, it is possible to get a couple of LT sectors having good latitudinal coverage on a single day, and hence, to get other LTs, one has to consider several days. We have considered multiple days from October only, to avoid the seasonal differences, if any. Yet we could not get very good LT coverage—there are

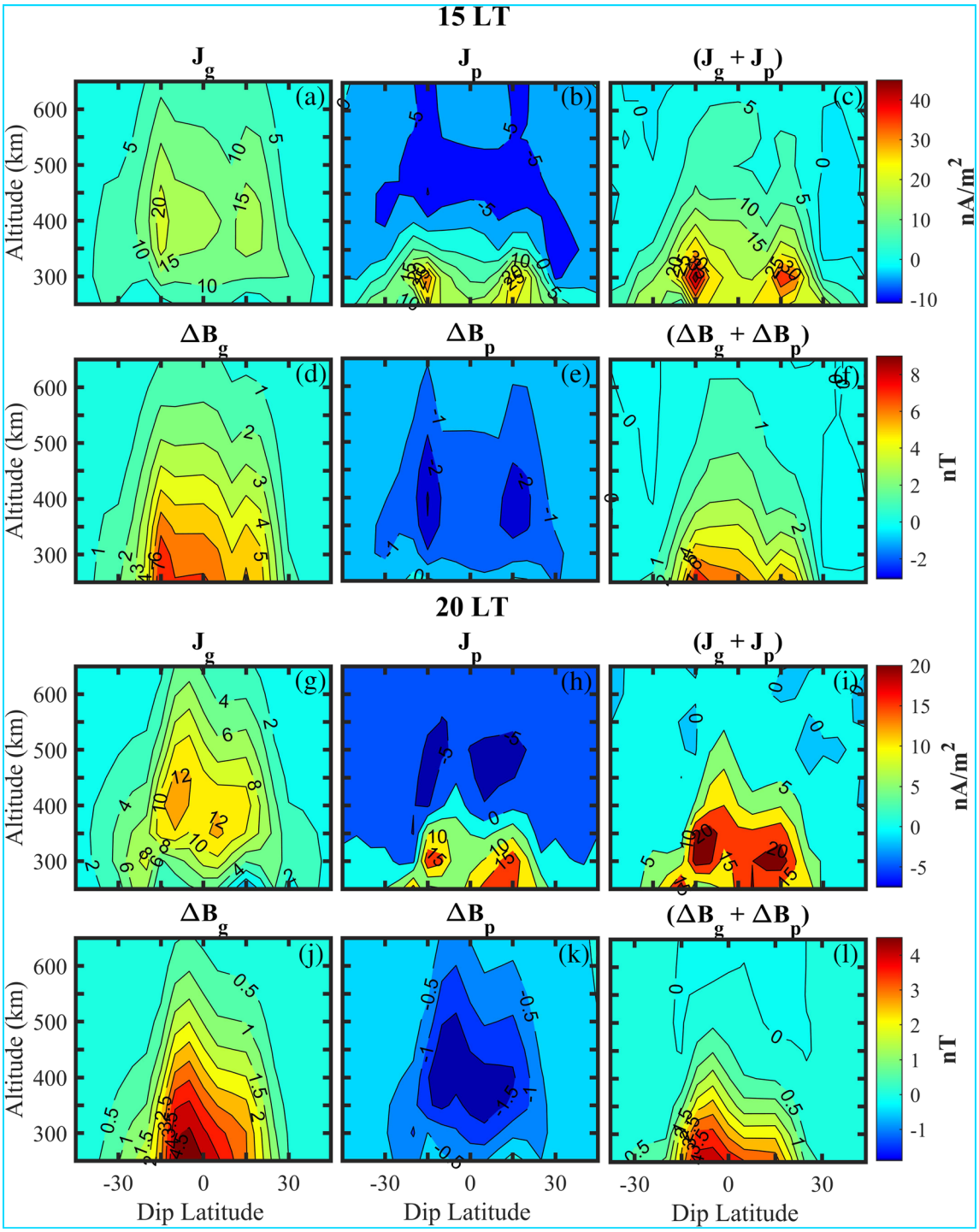

Figure 5. (a–c) Zonal currents due to gravity (J_g), pressure-gradients (J_p), and combined currents ($J_g + J_p$) and (d–f) their corresponding variations in the scalar magnetic field (ΔB_g, ΔB_p, and $\Delta B_g + \Delta B_p$) at 15 LT on 27 Sept 2014. (g–l) The same as (a)–(f) but at 20 LT.

empty sectors near 1, 7, 14, and 19 LT. In particular, the data gaps near 14 and 19 LT sectors are of concern, as the currents may be significant in those sectors. Table S1 shows the different dates and corresponding LT sectors used here to calculate the LT pattern. From the table, we can see that on some days there are only a couple of LT sectors with good latitudinal coverage. So, there are days providing as small as two LT sectors, while on some other days, it is eight. None of the days could provide all the local times. The average of the magnetic field perturbations is considered when the same LT sector is available multiple times.

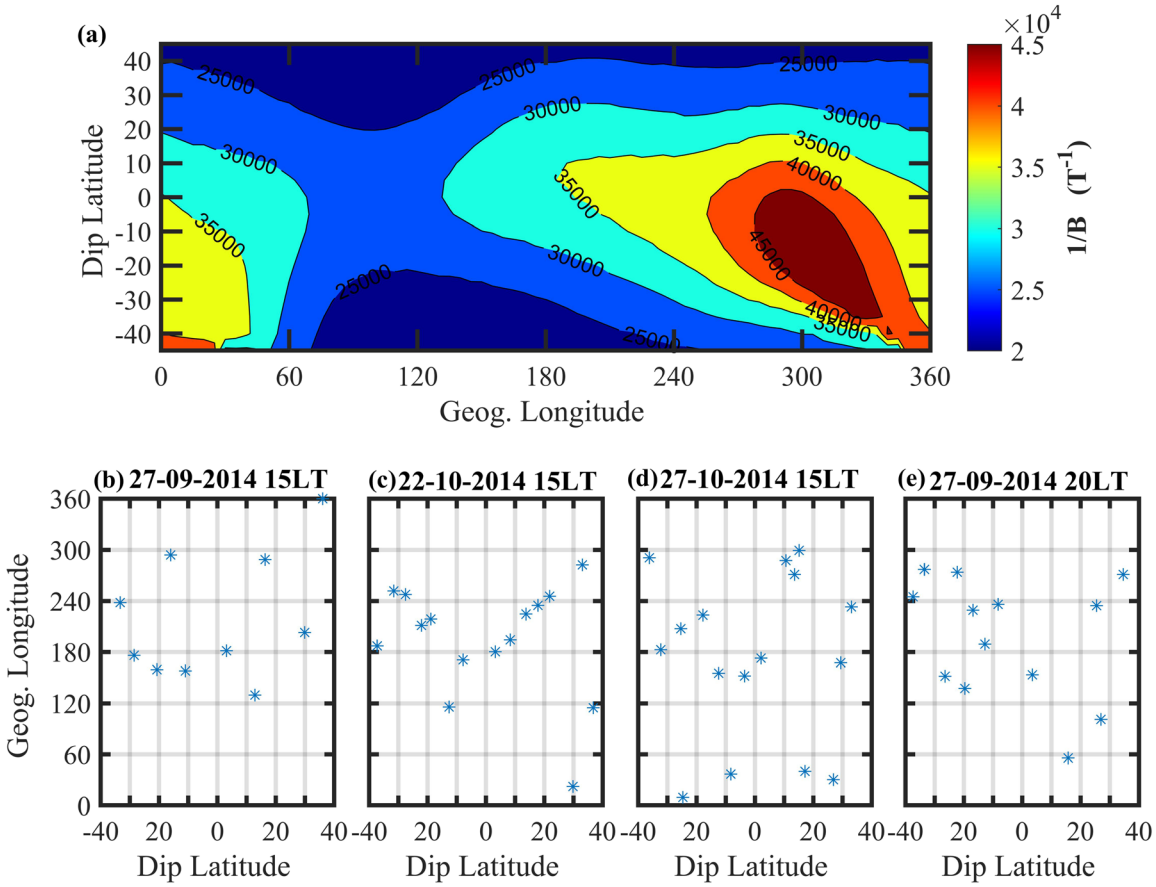

Figure 6. (a) Variation of reciprocal of the ambient magnetic field (1/*B*) shown in the longitude-dip latitude frame at an altitude of 300 km. (b–e) Longitudes of various occultation points used to obtain the latitudinal profiles on different days and LTs.

Figure 7 illustrates the latitudinal profiles of the magnetic field variations at different LTs, at the altitudes of 300 and 450 km. It is found that ΔB_g is positive and shows maxima near 15 LT with a magnitude ~6–8 nT at 300 km and 3–5 nT at 450 km in the dip equatorial-to-low-latitude region. ΔB_p is negative and shows peaks in the morning (around 10 LT) as well as in the afternoon hours (16–17 LT), at both altitudes (300 and 450 km). The magnitude of these peaks is ~3 nT. The net magnetic field variations shown in the rightmost columns reveal that the maximum amplitude of ($\Delta B_g + \Delta B_p$) is ~6–7 nT near the dip equatorial-to-low-latitude region at ~15–16 LT at 300 km and decreases to 3–4 nT at the altitude of 450 km. However, one should note that these patterns are approximate and may vary with different data points, as demonstrated in section 3.4.2 that mixing longitudes can significantly change these patterns. Since the latitudinal patterns displayed in Figure 7 at different LTs have used different number of days, one can compute the standard deviations to estimate the associated variability. We found (not shown here) that the standard deviation is mostly less than ~0.5 nT, except near 15 LT where it varies from 2 to 3.5 nT. However, one should keep in mind that these deviations are indicative of only day-to-day variability and do not account for the variability due to mixing of longitudes.

4. Discussions

In addition to the ionospheric-dynamo currents, the gravity and plasma pressure-gradient currents flow in the Earth's ionosphere, whose contribution on the ground is negligible compared to that of ionospheric-dynamo. However, these currents and the associated magnetic perturbation are important within the ionosphere and were estimated before, either using some approximations or based on models. Some studies have interpreted the night-time residual magnetic fields obtained from CHAMP and Swarm satellite observations, in terms of the signatures of GC and PC (Alken, 2016). The present work aims to estimate these currents using

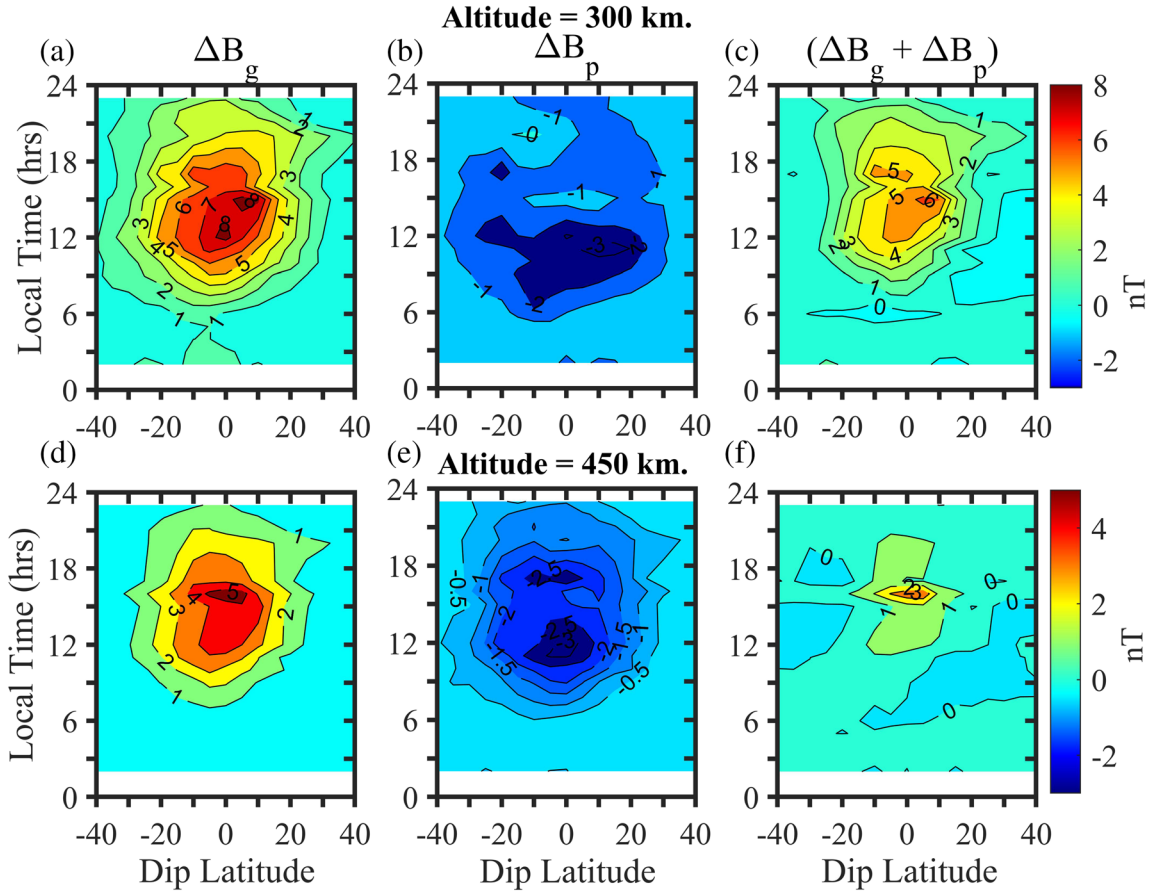

Figure 7. (a–f) The local time structure of ΔB_g, ΔB_p, and (ΔB_g + ΔB_p) at 300 and 450 km in the top and bottom panels, respectively, for October month.

COSMIC observations. Since LEO satellites fly in the ionosphere, which is the source region of GC and PC, it is important to know the magnetic field variations due to these currents. Computations of these currents using Equations 3 and 4 and their corresponding magnetic field variations using Equations 7 and 8 require the information of the entire height profile of the ionospheric plasma (including density, ion composition, and plasma temperatures), which is not available with LEO satellites. The approximation for estimating the magnetic field perturbation due to PC given by Lühr et al. (2003) has been used widely while analyzing the magnetic field measurements recorded by polar LEO satellites. The estimates obtained from the general circulation models (GCMs) have revealed that above the *F* region peak, the GC and PC are opposite in direction, and hence, net effect due to these currents is nonsignificant there (Maute & Richmond, 2017). They further suggested that correcting for only one current is not appropriate, as it may introduce errors of similar size as the observations (residual fields obtained after subtracting the main magnetic field) itself. In this context, it becomes imperative to estimate and understand the combined effects using actual observations. Through this paper, we intend to verify this aspect using actual electron density data collected by COSMIC satellite constellation. In the view of tremendous magnetic field data collected by the ongoing Swarm mission satellites, it is very important to clarify this point using actual electron density values at different local times, solar flux values, latitudes, and altitudes. Further, the purpose of the present work also includes, if possible, to obtain the estimates of magnetic field variations, which can be applied as the corrections to the satellite observations flying in different LT sectors.

The instruments deployed on the six microsatellites of COSMIC constellation provide the height profiles of the ionospheric electron density (Rocken et al., 2004), which has been used in the present study. Though the Abel inversion technique is widely used in GPS IRO, it often generates the artificial plasma cave (Liu et al., 2010; Yue et al., 2010) and results in unphysical negative electron densities at *E* region altitudes. Therefore, the electron densities at the lower heights are often not reliable, and hence the

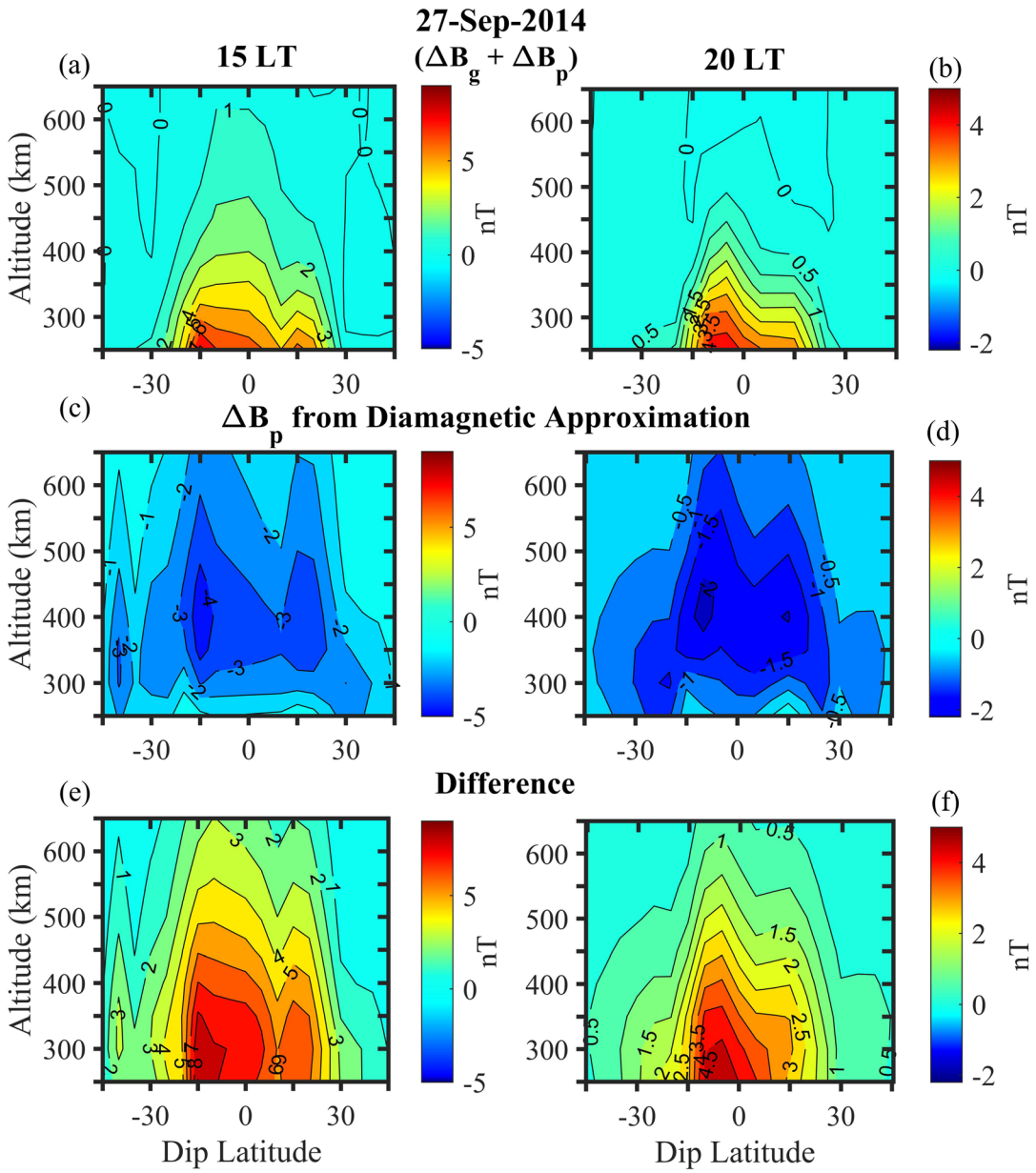

Figure 8. (a–f) Comparison between our results of ($\Delta B_g + \Delta B_p$) and ΔB_p from diamagnetic approximation on 27 September 2014 at 15 and 20 LT.

present study has considered the electron densities at the heights mainly above 200–250 km and computes the currents and magnetic field variations therein. Since LEO satellites normally fly between 300 and 700 km altitude, focusing on the altitudes above 250 km is suitable for the present study.

Maute and Richmond (2017) have comprehensively examined the magnetic signal due to gravity and plasma pressure-gradients using TIE-GCM simulations at 300°E longitude. To ease the comparison, we have also attempted to obtain the results at 300°E. In the present work, we use Equations 3 and 4 to compute $\boldsymbol{J}_g$ and $\boldsymbol{J}_p$ and ignore the currents produced by the induced electric fields. This can be a fair consideration, as at the altitude range of our interest the secondary Pedersen currents due to induced electric fields are negligible. The associated magnetic field variations are calculated based on the approximation of a one-dimensional current shell with zero height integrated current. Maute and Richmond (2017) have compared the magnetic field perturbations obtained with and without consideration of the induced electric fields. Their Figures 11-1b and 11-2b show the magnetic field variations due to GC obtained from the approximation shown by equation 7 here, and their Figures 11-1c and 11-2c are from a full three-dimensional current

system. The differences between these two estimates shown in their Figures 11-1d and 11-2d reveal that the approximation works in most of the region. At 15 LT, the differences are largest at lower altitudes <200 km and near dip equator. At 20 LT, the differences are prominent near 30°S geographic latitude below 300 km, and very small over all the other latitudes and altitudes. Thus, the approximation, which is much simpler to use compared to a full three-dimensional solution is suitable within an error of 1–2 nT in the region of our interest where LEO satellites normally fly.

Since the motive of the study is to obtain the magnetic field variations due to these currents at the altitudes of polar LEO satellites, it is required to get the latitudinal profile of these estimates at a fixed LT. However, sparsely available COSMIC data at different latitudes with fixed longitude and LT compels in compromising either for several days or different longitudes. Therefore, we have adopted the following two approaches: One is by considering different days to get the latitudinal profiles at a fixed longitude and LT; and the other approach is considering all the longitudes on a given day and LT. Both these approaches have some limitations of either mixing day-to-day variability or mixing different longitudes. As demonstrated in Figure 6a, the ambient magnetic field at different longitudes can modify the current computations considerably.

The results depicted in Figures 2, 3, and 5 indicate that the magnetic field variations due to GC and PC are important only at the dip equator-to-low latitude region, and magnetic fields are negligibly small poleward of 35° latitudes. Results obtained separately for GC and PC help to understand the relative and the net contributions of these currents. The net currents ($\boldsymbol{J}_g + \boldsymbol{J}_p$) and associated magnetic field variations ($\Delta B_g + \Delta B_p$) are stronger in the lower ionosphere and reduce considerably in the upper ionosphere. Figure 3 demonstrates that the currents ($\boldsymbol{J}_g$, $\boldsymbol{J}_p$) and magnetic field variations (ΔB_g, ΔB_p) increase almost linearly with the solar flux values, and are significant during higher solar flux conditions. At 15 LT over 300°E longitude, during the moderate solar flux, the net effect is found to be ~4.3 and 0.7 nT at 300 and 450 km height, respectively. And at low solar flux, it is as low as close to 0. During high solar flux, the ($\Delta B_g + \Delta B_p$) values are ~7 and 2 nT at 300 and 450 km height, respectively. Therefore, to understand the maximum extent of the effects of these currents, we have carried out the analysis for the high solar flux index ($F10.7 > 180$).

The eastward J_g is found to exhibit peaks in both the hemispheres at ~350–400 km altitude with a magnitude of ~20–30 nA/m^2, whereas ΔB_g is maximum at the lower altitudes and decreases with height. The eastward J_p shows peaks at ~300 km in both the hemispheres at ~ ±15° dip latitude, with an amplitude of 30 nA/m^2 at 15 LT and ~20 nA/m^2 at 20 LT. The westward J_p also shows peaks in both the hemispheres at ~500 km with amplitudes of ~10 nA/m^2 at 15 LT and ~5 nA/m^2 at 20 LT. The ΔB_p is southward with two peaks at ~ ±15° at an altitude of 400 km with a magnitude of ~1–3 nT. The ($J_g + J_p$) shows peaks in both the hemispheres at ~300 km with an amplitude of ~40–45 nA/m^2 at 15 LT and ~20 nA/m^2 at 20 LT. While ($\Delta B_g + \Delta B_p$) is largest at the lower altitudes (at 250 km, ~9 and ~5 nT at 15 and 20 LT, respectively) and decreases with height (at 450 km, ~2.2 nT 15 LT and <1 nT at 20 LT). It has a very weak two-peak pattern, which disappears at higher altitudes. As the magnitude and altitude variation of the current density depends very much on the electron density profile (e.g., the height and peak density of the *F* layer), we examined the differences between the electron density profiles obtained by COSMIC observations and TIE-GCM. It is found that the TIE-GCM plasma densities displayed in Maute and Richmond (2017) are stronger and peak at higher altitudes compared to those obtained from COSMIC observations. Hence, the lower magnitudes and lower altitudes of the current densities obtained here are apparent. The broad features of our results agree with the results presented by Maute and Richmond (2017).

The latitudinal patterns at different local times displayed in Figure 7 for the *F* region altitudes have shown that the magnetic field effects vary at different LT sectors and are significant in the noon to evening sector. The intention behind making these latitudinal profiles at different LTs is obtaining the corrections in the magnetic field observations recorded by the LEO satellite magnetometers flying in the *F* region. However, one should note that the patterns displayed in Figure 7 are approximate and may vary with different data points, as demonstrated in section 3.4.2 that mixing longitudes can significantly change these patterns. The patterns can be obtained using the first approach as well, which is for the fixed longitude. But this approach requires many days with geomagnetic quiet conditions, similar months and solar flux values. From the time of launch of the COSMIC constellation in 2006 till now, getting days with high solar flux is very limited. Therefore, obtaining these corrections using COSMIC observations, for high solar flux when the corrections can be important, is not feasible in the near future. It would need observations from a

relatively stronger solar cycle period. However, getting the patterns during low to moderate solar flux values is possible. In the future, the electron density profiles based on some empirical model can be used for getting these corrections.

Alken (2016) used residual magnetic fields obtained from LEO satellite observations for studying the signatures of GC and PC. As the residual fields would contain the effects due to both these currents, they used the orientations of the vector components of the residual fields to speculate about the dominance of either $\boldsymbol{J}_g$ or $\boldsymbol{J}_p$ currents. They reported that these currents can produce perturbations of one to a few nT in LEO satellite measurements, even up to midnight during both solar maximum and minimum. However, according to the present analysis during high solar flux, only 1–2 nT variations can be present until midnight at 300 km altitude and almost no magnetic field variation after 21 LT at 450 km.

Figure 8 compares $(\Delta B_g + \Delta B_p)$ values obtained using Equations 7 and 8 (upper panel) with the magnetic field correction applied using diamagnetic approximation $(\Delta B_{p\mathrm{Appx}})$ from Lühr et al. (2003) (middle panel), on a fixed day of 27 September 2014 at 15 and 20 LT. The differences between these two values are shown in the bottom panel. From the figure, it is clear that both the magnetic field corrections are different in magnitude and also direction. The $(\Delta B_g + \Delta B_p)$ are mainly northward with a maximum amplitude of ~6 nT at lower altitudes below 300 km. Contrarily, $(\Delta B_{p\mathrm{Appx}})$ is essentially southward with maximum amplitude close to 4 nT. At an altitude of 450 km, over the dip equator, $(\Delta B_g + \Delta B_p)$ indicates correction of ~−2.2 nT, while $(\Delta B_{p\mathrm{Appx}})$ suggests a correction of ~ +3 nT, and consequently, there is a net difference of ~5 nT between these two values. Thus, the correction based on the diamagnetic approximation is in the opposite direction with an almost similar range of magnitude, which would result in almost doubling the error in the correction. This indicates that the correction of only one current instead of considering the combined effects of $(\Delta B_g + \Delta B_p)$ would introduce unnecessary errors, and hence, it is advisable not to apply any correction at all rather than correction of only one current component. As stated above, it is not possible to estimate ΔB_g based on the data collected by the onboard LEO instruments, and hence the possibility of estimating it using inflight data is absent until some approximation for ΔB_g is worked out.

5. Conclusions

Using the vertical profiles of the ionospheric electron densities obtained from COSMIC-1 satellite cluster, the following conclusions are drawn:

1. Using COSMIC data, it is not possible to get good latitudinal coverage of ionospheric electron density profiles on a given day at a fixed LT and longitude, as required by LEO satellite trajectories. Hence, fails to reproduce the standard electron density patterns in the latitude-altitude frame, missing the EIA features.
2. Therefore, one has to compromise either with days or longitudes, that is, need to consider either several days at a fixed longitude or different longitudes on a fixed day.
3. The magnetic field variations due to gravity and pressure-gradient currents $(\Delta B_g + \Delta B_p)$ are important only at the dip equator to low-latitude region, and fields are negligibly small beyond 35° latitudes.
4. The magnetic field variations $(\Delta B_g + \Delta B_p)$ are stronger in the lower ionosphere and reduce considerably in the upper ionosphere.
5. The effects of GC and PC increase almost linearly with the solar flux values and are significant during higher solar flux conditions.
6. The magnetic field effects of these currents vary at different LT sectors, which are significant in the noon to evening sector, and negligibly small in other LT sectors.
7. To apply the corrections due to these currents in the magnetic measurements recorded by the LEO satellites, the latitudinal profiles are obtained at different LTs. However, during high solar activity, it was possible to obtain these patterns only by ignoring the longitudinal differences. Hence, there is a need to use either COSMIC data-based empirical model values for electron density profiles or get the patterns from full three-dimensional solutions through general circulation models.
8. The study demonstrates that correcting the LEO satellite magnetic measurements for only one current such as PC through diamagnetic approximation can introduce unnecessary errors.
9. The present study suggests that there is no need of correction for GC and PC in the magnetic field measurements by the LEO satellite if

i. the satellite orbit is above 700 km,
ii. the satellite orbit is during night to morning times, and
iii. the satellite traverses during a period of low solar flux.

Data Availability Statement

The F3/C data are obtained from UCAR-CDAAC (http://cdaac-www.cosmic.ucar.edu/cdaac/products.html), which are available in the public domain. The data have been taken from "COSMIC" mission and "ionPrf" product. The geomagnetic activity index Kp was provided by the GFZ German Research Centre for Geosciences (https://www.gfz-potsdam.de/en/kp-index/). The solar activity index F10.7 was downloaded from SPDF OMNIWeb database (https://omniweb.gsfc.nasa.gov/form/dx1.html).

Acknowledgments
This work is supported by the Department of Science and Technology, Government of India. We are grateful to Taiwan's National Space Organization (NSPO) and the University Corporation for Atmospheric Research (UCAR) for making the F3/COSMIC data available. Authors thank Tulasi Ram and Sai Gowtam for their help in understanding the COSMIC data.

References

Alken, P. (2016). Observations and modeling of the ionospheric gravity and diamagnetic current systems from CHAMP and Swarm measurements. *Journal of Geophysical Research: Space Physics*, *121*, 589–601. https://doi.org/10.1002/2015JA022163

Alken, P., Maus, S., Richmond, A. D., & Maute, A. (2011). The ionospheric gravity and diamagnetic current systems. *Journal of Geophysical Research*, *116*, A12316. https://doi.org/10.1029/2011JA017126

Alken, P., Maute, A., & Richmond, A. D. (2017). The *F*-region gravity and pressure gradient current systems: A review. *Space Science Reviews*, *206*(1–4), 451–469. https://doi.org/10.1007/s11214-016-0266-z

Bilitza, D., Altadill, D., Truhlik, V., Shubin, V., Galkin, I., Reinisch, B., & Huang, X. (2017). International Reference Ionosphere 2016: From ionospheric climate to real-time weather predictions. *Space Weather*, *15*, 418–429. https://doi.org/10.1002/2016SW001593

Cheng, C.-Z. F., Kuo, Y.-H., Anthes, R. A., & Wu, L. (2006). Satellite constellation monitors global and space weather. *Eos, Transactions American Geophysical Union*, *87*(17), 166. https://doi.org/10.1029/2006EO170003

Chulliat, A., Vigneron, P., & Hulot, G. (2016). First results from the Swarm Dedicated Ionospheric Field Inversion chain. *Earth, Planets and Space*, *68*(1), 104. https://doi.org/10.1186/s40623-016-0481-6

Finlay, C. C., Olsen, N., Kotsiaros, S., Gillet, N., & Toffner-Clausen, L. (2016). Recent geomagnetic secular variation from *Swarm* and ground observatories as estimated in the CHAOS-6 geomagnetic field model. *Earth, Planets and Space*, *68*(1), 112. https://doi.org/10.1186/s40623-016-0486-1

Hulot, G., Sabaka, T., Olsen, N., & Fournier, A. (2015). The present and future geomagnetic field. In *Treatise on geophysics* (2nd ed., pp. 33–78). Amsterdam/San Diego: Elsevier/Academic Press.

Jadhav, G., Rajaram, M., & Rajaram, R. (2002a). A detailed study of equatorial electrojet phenomenon using Ørsted satellite observations. *Journal of Geophysical Research*, *107*(A8), 1175. https://doi.org/10.1029/2001JA000183

Jadhav, G., Rajaram, M., & Rajaram, R. (2002b). Main field control of the equatorial electrojet: A preliminary study from the Oersted data. *Journal of Geodynamics*, *33*(1–2), 157–171. https://doi.org/10.1016/S0264-3707(01)00061-8

Liu, J. Y., Lin, C. Y., Lin, C. H., Tsai, H. F., Solomon, S. C., Sun, Y. Y., et al. (2010). Artificial plasma cave in the low-latitude ionosphere results from the radio occultation inversion of the FORMOSAT-3/COSMIC. *Journal of Geophysical Research*, *115*, A07319. https://doi.org/10.1029/2009JA015079

Lühr, H., & Maus, S. (2006). Direct observation of the F region dynamo currents and the spatial structure of the EEJ by CHAMP. *Geophysical Research Letters*, *33*, L24102. https://doi.org/10.1029/2006GL028374

Lühr, H., Maus, S., & Rother, M. (2004). Noon-time equatorial electrojet: Its spatial features as determined by the CHAMP satellite. *Journal of Geophysical Research*, *109*, A01306. https://doi.org/10.1029/2002JA009656

Lühr, H., Maus, S., Rother, M., & Cooke, D. (2002). First in-situ observation of night-time *F* region currents with the CHAMP satellite. *Geophysical Research Letters*, *29*(10), 1489. https://doi.org/10.1029/2001GL013845

Lühr, H., Rother, M., Maus, S., Mai, W., & Cooke, D. (2003). The diamagnetic effect of the equatorial Appleton anomaly: Its characteristics and impact on geomagnetic field modeling. *Geophysical Research Letters*, *30*(17), 1906. https://doi.org/10.1029/2003GL017407

Maeda, K.-I. (1981). Internal structure of the equatorial ionospheric dynamo. *Journal of Atmospheric and Terrestrial Physics*, *43*(5–6), 393–401. https://doi.org/10.1016/0021-9169(81)90103-3

Manoj, C., Lühr, H., Maus, S., & Nagarajan, N. (2006). Evidence for short spatial correlation lengths of the noontime equatorial electrojet inferred from a comparison of satellite and ground magnetic data. *Journal of Geophysical Research*, *111*, A11312. https://doi.org/10.1029/2006JA011855

Maus, S., & Lühr, H. (2006). A gravity-driven electric current in the Earth's ionosphere identified in CHAMP satellite magnetic measurements. *Geophysical Research Letters*, *33*, L02812. https://doi.org/10.1029/2005GL024436

Maus, S., Yin, F., Lühr, H., Manoj, C., Rother, M., Rauberg, J., et al. (2008). Resolution of direction of oceanic magnetic lineations by the sixth-generation lithospheric magnetic field model from CHAMP satellite magnetic measurements. *Geochemistry, Geophysics, Geosystems*, *9*, Q07021. https://doi.org/10.1029/2008GC001949

Maute, A., & Richmond, A. D. (2017). Examining the magnetic signal due to gravity and plasma pressure gradient current with the TIE-GCM. *Journal of Geophysical Research: Space Physics*, *122*, 12,486–12,504. https://doi.org/10.1002/2017JA024841

Pedatella, N. M., Yue, X., & Schreiner, W. S. (2015). An improved inversion for FORMOSAT-3/COSMIC ionosphere electron density profiles. *Journal of Geophysical Research: Space Physics*, *120*, 8942–8953. https://doi.org/10.1002/2015JA021704

Rocken, C., Kuo, Y.-H., Sokolovskiy, S. V., & Anthes, R. A. (2004). The ROCSAT-3/COSMIC mission and applications of GPS radio occultation data to weather and climate. *Remote Sensing Applications of the Global Positioning System*, *5661*, 1–12. https://doi.org/10.1117/12.566544

Schreiner, W., Rocken, C., Sokolovskiy, S., Syndergaard, S., & Hunt, D. (2007). Estimates of the precision of GPS radio occultations from the COSMIC/FORMOSAT-3 mission. *Geophysical Research Letters*, *34*, L04808. https://doi.org/10.1029/2006GL027557

Singh, D., Gurubaran, S., & He, M. (2018). Evidence for the influence of DE3 tide on the occurrence of equatorial counterelectrojet. *Geophysical Research Letters*, *45*, 2145–2150. https://doi.org/10.1002/2018GL077076

Sugiura, M., & Hagan, M. P. (1979). Geomagnetic Sq variation at satellite altitudes: Is Sq correction important in Magsat data analysis? *Geophysical Research Letters*, *6*(5), 397–400. https://doi.org/10.1029/GL006i005p00397

Thébault, E., Lesur, V., Kauristie, K., & Shore, R. (2017). Magnetic field data correction in space for modelling the lithospheric magnetic field. *Space Science Reviews*, *206*(1–4), 191–223. https://doi.org/10.1007/s11214-016-0309-5

Thomas, N., Vichare, G., & Sinha, A. K. (2017). Characteristics of equatorial electrojet derived from Swarm satellites. *Advances in Space Research*, *59*(6), 1526–1538. https://doi.org/10.1016/j.asr.2016.12.019

Tulasi Ram, S., Su, S., Tsai, L., & Liu, C. H. (2016). A self-contained GIM-aided Abel retrieval method to improve GNSS-Radio Occultation retrieved electron density profiles. *GPS Solutions*, *20*(4), 825–836. https://doi.org/10.1007/s10291-015-0491-z

Vichare, G., & Rajaram, R. (2011). Global features of quiet time counterelectrojet observed by Ørsted. *Journal of Geophysical Research*, *116*, A04306. https://doi.org/10.1029/2009JA015244

Yue, X., Schreiner, W. S., Lei, J., Sokolovskiy, S. V., Rocken, C., Hunt, D. C., & Kuo, Y.-H. (2010). Error analysis of Abel retrieved electron density profiles from radio occultation measurements. *Annales Geophysicae*, *28*(1), 217–222. https://doi.org/10.5194/angeo-28-217-2010